HHS Public Access

Author manuscript

Acad Radiol. Author manuscript; available in PMC 2023 September 10.

Published in final edited form as:

Acad Radiol. 2022 November ; 29(11): 1623–1630. doi:10.1016/j.acra.2022.01.008.

Visualization and validation of the microstructures in the airway wall *in vivo* using diffractive optical coherence tomography

Jeffrey Thiboutot[1,*], **Wu Yuan**[2,3,*], **Hyeon-cheol Park**[2], **Dawei Li**[2], **Jeffrey Loube**[4], **Wayne Mitzner**[1,4,5], **Lonny Yarmus**[1], **Xingde Li**[2,#], **Robert H. Brown**[1,4,5,#]

[1]Division of Pulmonary and Critical Care Medicine, School of Medicine, Johns Hopkins University, Baltimore, MD 21205, USA.

[2]Department of Biomedical Engineering, School of Medicine, Johns Hopkins University, Baltimore, MD 21205, USA.

[3]Department of Biomedical Engineering and Shun Hing Institute of Advanced Engineering, The Chinese University of Hong Kong, Hong Kong SAR, China.

[4]Department of Environmental Health and Engineering, Bloomberg School of Public Health, Johns Hopkins University, Baltimore, MD 21205, USA.

[5]Department of Anesthesiology/Critical Care Medicine, School of Medicine, Johns Hopkins University, Baltimore, MD 21205, USA.

Abstract

Rationale and Objectives: At present, there is no available method to study the *in vivo* microstructures of the airway wall (epithelium, smooth muscle, adventitia, basement membrane, glands, cartilage). Currently, we rely on *ex vivo* histologic evaluation of airway biopsies. To overcome this obstacle, we have developed an endoscopic ultrahigh-resolution diffractive optical coherence tomography (OCT) system, operating at a wavelength of 800 nm, to non-invasively study the *in vivo* microstructures of the airway wall. Prior to human study, validation of diffractive OCT's ability to quantitate airway microstructural components is required.

Materials and Methods: To validate and demonstrate the accuracy of this OCT system, we used an ovine model to image small airways (~ 2 mm in diameter). Histologic samples and correlated OCT images were matched. The cross-sectional area of the airway wall, lumen, and other microstructures were measured and compared.

Send correspondence to: Robert H. Brown, MD, MPH, 615 N. Wolfe St, Department of Environmental Health and Engineering, Room E7614, Baltimore, Maryland, 21205, phone: 410-614-5451, rbrown@jhsph.edu.

*These authors have contributed equally to this work

#These authors have contributed equally to this work

Author contributions: X.D.L. and R.H.B. conceived the idea, designed studies. W.Y., H.P. and D.L. developed and characterized the diffractive OCT catheter and system. W.Y., J.T., H.P., J.L., R.H.B. and W.M. performed the studies. R.H.B., W.Y., J.T. and W.M. correlated the histology with OCT results. W.Y. and J.T. labeled OCT images. R.H.B. and J.T. performed the statistical analysis and labeled histology. X.D.L. supervised the theoretical and experimental works. All authors contributed to the manuscript preparation.

Competing interests: The authors declare that they have no competing interests.

Results: A total of 27 sheep were studied from which we identified 39 paired OCT–histology airway images. We found strong correlations between the OCT and the histology measurements of the airway wall area and the microstructural area measurements of the epithelium, basement membrane, airway smooth muscle, glands, cartilage, and adventitia. The correlations ranged from r=0.61 (p<0.001) for the epithelium to r=0.86 (p<0.001) for the adventitia with the correlation between the OCT and the histology measurements for the entire airway wall of r=0.76 (p<0.001).

Conclusion: Given the high degree of correlation, these data validate the ability to acquire and quantify *in vivo* microscopic level imaging with this newly developed 800nm ultra-high resolution diffractive OCT system.

Introduction

The most common means of evaluating the lungs is by indirect methods such as auscultation and pulmonary function testing. Direct imaging technology can improve our understanding of pathophysiological changes in the lungs. A standard Chest X-Ray (CXR) has been available for over a century. However, it is limited to identifying gross changes such as pulmonary edema, infiltrative processes, or severe emphysematous changes. Over the past several decades, additional imaging methods capable of more direct assessment of the anatomy of the lungs have become available. The most commonly used advanced imaging technology to evaluate pulmonary anatomy is Computed Tomography (CT). CT can measure changes in the parenchyma, the airways, and the vessels. However, CT does not have the resolution to visualize the microstructural components of the airways or parenchyma.

Currently, the most common method to evaluate the microstructures of the airway wall is through histologic assessment of biopsy specimens, either obtained bronchoscopically or through surgical resection. The critical site of disease for many pulmonary diseases is found in the microstructures of the airways, for example in the epithelium, airway smooth muscle, glands, and basement membrane. A non-invasive method to visualize and quantify changes in these microstructures is critical to improve our ability to assess severity, response to treatment, and prognostication for pulmonary diseases such as asthma, COPD, cystic fibrosis, and interstitial lung disease.

Endoscopic optical coherence tomography (OCT) is a technology capable of *in vivo* imaging of internal luminal organs non-invasively with micron-scale resolution and without ionizing radiation(5, 20, 26). Endoscopic OCT provides near histologic quality visualization of tissue microstructures and allows volumetric sampling over a large area(26). Recent advancements in catheter design have greatly expanded the potential of endoscopic OCT to a wide range of clinical applications(8, 14, 18, 23, 24). Initial use of 1300-nm endoscopic OCT has demonstrated the potential utility of measuring airway wall thickness in patients(3, 4). More recently, birefringence OCT has been used to detect pathologic airway remodeling in people with asthma with the ability to assess airway smooth muscle (ASM) *in vivo* (1, 2). This birefringence OCT system operating at 1300 nm, utilizes polarized reflection of light to highlight ordered structures visualized with OCT such as smooth muscle bundle fibers. However, this technology was suboptimal for accurately imaging other non-ordered structural components within the airway wall. This was mainly due to the limited resolution

(about 10 μm) and imaging contrast afforded by conventional endoscopic OCT operating at 1300 nm. To address these limitations of traditional OCT, a 800-nm diffractive OCT endoscopy has been recently developed to provide higher resolution and improved image contrast for multiple airway wall structures(15, 22, 25).

The current study was performed to demonstrate the accuracy and validity of ultrahigh-resolution 800-nm diffractive OCT system to visualize multiple microstructures in small airways in an ovine model. We identified specific airway segments, measured the structural components of the airway wall (i.e. epithelium, glands, ASM, cartilage), and compared these to matched histology at the same location in the airway. The capability of 800-nm diffractive OCT image to delineate and quantify the structural components of the airway wall provides an opportunity to explore aspects of airway morphology *in vivo* and may serve as a future tool to elucidate the pathophysiology of human lung disease.

Materials and Methods

Preclinical model

The following animal protocol in an ovine model was approved by the Animal Care and Use Committee of the Johns Hopkins University. Anesthesia was initiated with intramuscular ketamine (25 mg kg^{-1}) and maintained with a continuous intravascular (IV) infusion of propofol (800 μg kg^{-1} h^{-1}). The trachea was intubated, and the animals were mechanically ventilated at 14 breaths per minute with a tidal volume adequate to maintain an end tidal carbon dioxide level of approximately 30 mmHg (23). To allow measurements in the smallest airways, a tracheostomy was then performed, and a shortened endotracheal tube was passed into the trachea and secured. A bronchoscope (Olympus BF-P40) was passed through the endotracheal tube into the sheep airways of the right middle lobe. The 800-nm diffractive OCT catheter was then passed through the 2.2-mm diameter working channel of the bronchoscope to a selected airway until gentle resistance was met.

Ultrahigh-resolution diffractive OCT system

Our group previously demonstrated the use of a diffractive lens in the OCT catheter design to overcome chromatic aberration(22). Based on that work, we further optimized the performance of the OCT catheters with custom diffractive optics to mitigate the chromatic aberration over the broad spectral bandwidth of about 200 nm centered around 800 nm (Figure 1a–b). The diffractive catheter maintained a smaller diameter of 1.3 mm including the encasing metal guard at its distal end. The overall diameter of the imaging probe was approximately 1.8 mm including the protective plastic sheath running along the entire length of the catheter, offering a measured lateral resolution of about 7.2μm (Figure 1c). To illustrate the achromatic performance of the diffractive catheter, we measured the back-reflected spectra by placing a mirror at different locations relative to the focal plane of the catheter. We found that the measured spectra remained nearly unchanged along the imaging depth (Figure 1d), confirming the achromaticity of the diffractive catheter, which was critical for achieving a consistent ultrahigh axial resolution afforded by the broadband light source(23). The improved diffractive OCT system offered an ultrahigh axial resolution of about 2.4μm in air (or 1.7μm in tissue) (Figure 1e).

A bench-top endoscopy system based on an 800-nm spectral-domain OCT (SD-OCT) platform was developed for imaging *in vivo* airways. The details of this SD-OCT system were reported previously(22, 25). In brief, it consisted of a home-built linear-k spectrometer of 2K pixels, which can accommodate a spectrum bandwidth of approximately 250 nm centered around 800 nm and offered an imaging depth of approximately 1.2 mm. A home-made Ti:sapphire laser with a center wavelength of about 820 nm and an 3dB spectral bandwidth of approximately 150 nm was used as well as a portable continuum laser. Catheter rotation speed up to 20 frames per second was performed by using an improved home-made broadband fiber-optics rotary joint, providing a one-way throughput >87%, an optical coupling variation < ±4% during continuous rotation, and a measured back-reflection < −58 dB(19). The catheter pullback rate was 0.4 mm/s, corresponding to an image-to-image pitch of approximately 20 μm. The imaging system achieved a detection sensitivity of −108 dB with a near-theoretical-limit sensitivity roll-off of approximately −13 dB/mm(22, 25). The acquired cross-sectional OCT images were converted to a logarithmic scale and displayed in an 8-bit gray scale with 1024×1024 pixels.

Tissue registration and histology correlation

Two methods were used to facilitate the identification of the airway segment for matching OCT images and histology slides. One method was to leave the plastic sheath that encased the OCT imaging catheter in the sheep airway. The catheter was located and immobilized in the imaged airway segment and removed with the lungs *en block*. The other method was to mark the imaged airway sections using a laser catheter made with an SMF28 fiber, delivering a 1,448-nm laser beam with a power of approximately 350 mW. This laser catheter was deployed to the imaging sites through the same plastic sheath which was used to host the imaging catheter. An exposure time of 10 seconds was used to make burn marks on the airway wall. The airway was imaged before and after the laser marking procedure (Figure 2). In addition, we measured the depth of the bronchoscope for each airway in each sheep and video recorded the path to the marked airway during in vivo imaging.

After OCT imaging was completed, the sheep were sacrificed and the lungs were removed *en block*, inflated to 25 cmH_2O, and fixed in 10% neutral buffered formalin for at least one week. After fixation, the fixative was drained by gravity. We used the video to guide us to the marked area in the ex vivo fixed lungs. A bronchoscope was passed into the *ex-vivo* lungs and the same airway locations that were imaged were identified and dissected. Following dissection of the imaged airway segments, histologic slides were prepared and stained with standard H&E and converted to micrographs (Figure 3). The histologic images were then manually matched to the corresponding OCT images. Microstructures and tissue compartments of small airways in cross-sectional OCT images and histology micrographs were labelled manually using Semantic segmentation editor, an open-sourced web-based interactive image annotation tool (Semantic segmentation editor. Hitachi Automotive and Industry Lab, 2019). The labeled cross-sectional OCT and histologic correlates were exported to MATLAB v9.5 (The MathWorks Inc, Massachusetts, United States). Using a pixel counting technique, the cross-sectional areas of the airway wall, airway lumen, and structural components (epithelium, basement membrane, smooth muscle, glands, adventitia and cartilage) were quantified.

Statistical analysis

Statistical analyses were performed using JMP (Version 11.0.0). Structural component areas measured by OCT and histology were compared using paired t-tests and a linear regression model with least squares optimization. P values less than or equal to 0.05 were considered statistically significant.

Results

A total 27 sheep were studied from which we identified 39 paired OCT – histology airway images. We were able to clearly identify the various structural components of the airway wall, including the epithelium, basement membrane, airway smooth muscle (ASM), adventitia, glands, cartilage, blood vessels, and alveoli. Figure 3 demonstrates an example of the OCT – histology paired images with the airway wall structural components identified.

Based on the size of the catheter and the set focal point of the OCT system, the imaged airways were approximately 1.8 mm in luminal diameter (the size of the OCT catheter and protective sheath). The mean airway luminal diameter was 2.6±0.39 mm (mean±SD) as measured on the OCT images and 1.8±0.97 mm as measured on histology ($p<0.0001$). The slightly smaller size on histology was likely due to changes secondary to the fixation and embedding processes. We also compared the average values for the total airway wall area and the structural components within the airway wall (Table 1). For the total wall area, we found a small but significant difference in the average wall areas on the OCT image compared to histology ($p=0.02$).

We also found small but significant differences in the area measurements of the epithelium ($p<0.001$), ASM ($p<0.001$), glands ($p<0.001$), and cartilage ($p=0.03$). To assess for any directionality of bias between the OCT imaging and histology, Bland-Altman plots were generated for each of the microstructures of the airway wall (Figure 4). We did not observe any systematic differences between the two measurements. For example, the measurement on OCT compared to histology for the epithelial area was slightly larger. In contrast, the measurement on OCT compared to histology for the cartilage area was slightly smaller. For some of the structural components, the basement membrane ($p=0.57$) and adventitia ($p=0.17$), we found no difference between the OCT and histology measurements.

Using linear regression across all airways, we also examined the correlation between the OCT and histology measurements for the airway wall and the structural components. We found strong correlations between the OCT and the histology measurements of the entire airway wall area as well as the measurements of the structural components: epithelium, basement membrane, ASM, glands, cartilage, and adventitia (Table 2). The correlations ranged from $r=0.61$ ($p<0.001$) for the epithelium to $r=0.86$ ($p<0.001$) for the adventitia with the correlation between the OCT and the histology measurements for the entire airway wall of $r=0.76$ ($p<0.001$).

Discussion

Our results demonstrate that we are able to image the microstructures of the airway wall *in vivo* with near micron scale resolution with our recently improved 800nm diffractive OCT system (22, 23, 25). These results validate the use of diffractive OCT to identify airway wall microstructures and document potential changes non-invasively. A validated method to image the airway wall and its structural components *in vivo* at the microscopic level opens the door to a multitude of diagnostic and prognostic possibilities.

Adams and colleagues were among the first to image the microstructures of the airway wall using OCT *in vivo*. In both animal and human models, they were able to identify and quantify ASM. Their approach capitalizes on the highly ordered structure of ASM which permits birefringence microscopy to identify and highlight the areas of ASM that were not immediately obvious via OCT imaging alone at 1300nm. This orientation resolved OCT imaging approach was a significant advancement that enabled the evaluation of pathologic airway smooth muscle remodeling in individuals with asthma. There have been few other published manuscripts validating pulmonary OCT imaging, and all were with a 1300nm wavelength. Chen et al. showed a reasonable concordance between the OCT and histology for the 6^{th} through the 9^{th} generation airways for their airway wall, airway luminal, and airway diameter measurements in humans(3). However, they were not able to measure the structural components within the airway wall with their 1300-nm OCT system. Lee et al. demonstrated good correlations between OCT and airway wall measurements(13). They divided the airway wall into three concentric areas within the wall as well as measuring the total wall area. While they showed strong correlations between the OCT and histology measurements, again using a 1300-nm OCT system, they were not able to differentiate the individual structural components within the airway wall. Hariri et al. showed OCT and matched histological images of airway structural components of an ex vivo airway(9). However, they did not present any measurements nor statistical analysis of the matched OCT and histological images. Adams et al. using a birefringence OCT system to measure the ASM showed a high correlation between OCT images and histology from both dogs and pig bronchioles(1). Our 800-nm system offers an increase in resolution that provides more granularity in visualization of all the microstructures in the airway wall.

The 800nm endoscopic OCT (15, 19, 21–23, 25), offers higher resolution and importantly improved image contrast designed to address the limitations of traditional 1300nm OCT. To overcome the severe chromatic aberration faced by the conventional GRIN-lens based micro-optics in OCT catheters when using a broad spectrum at 800nm, a diffractive catheter design was previously proposed by our group(22).

Compared to the first report on an 800nm endoscopic OCT system back in 2014, the one used in the current airway imaging study has been improved considerably in terms of resolution, signal to noise ratio, and system portability(16, 19, 25). In addition, we further minimize the size of OCT catheter from 2.1 mm to 1.8 mm (Figure 1.a–c) allowing it to be used with and passed through the working channel of a standard clinical bronchoscope. We also further optimized the performance of the system on achromaticity (Figure 1.d) and axial resolution (Figure 1.e). Our 800nm endoscopic diffractive OCT system offers super-

achromatic performance, achieving 1.7μm imaging resolution (in tissue) which represents a 4X improvement over conventional 1300nm OCT. As this diffractive OCT enables high-definition visualization of multiple microstructures of the airway, it does not rely on birefringence microscopy to highlight ordered structures (e.g. ASM).

While we did not observe any systematic difference between the histology and OCT measurements, quantitative differences did exist despite good correlation. There are likely two competing factors driving these findings. First is shrinkage artifact that is induced with histologic preparation (with potential bias decreasing histologic quantification). We did make efforts to fix the lungs while inflated to 25 cmH_2O. However, this likely will only marginally mitigate shrinkage. Second is a decrease in quantification of OCT microstructure that is induced by conservative labeling of the structures. While the 800-nm system does provide high quality images, the quality is still less than that of histology, meaning OCT imaging may miss subtleties of the microstructures leading to underestimates of their volume. As both histology shrinking and OCT underestimates occur in the same direction, this likely accounts to the lack of systemic bias in any one direction.

With real-time imaging of the airways, diagnosis of several pulmonary diseases could become more accurate. For example, it is known that patients who die of an acute asthma attack have significantly more airway smooth muscle(6, 11). However, there is currently no way of identifying such asthmatic patients and thereby determining who is at greatest risk. OCT could be used to determine which asthmatic patients have increased airway smooth muscle and are at risk of sudden death. Another potential diagnostic use of OCT is to determine which patients with severe asthma would respond to bronchial thermoplasty (BT). Since the proposed mechanism of BT is destruction of the ASM, OCT could enable the selection of patients with the greatest burden of ASM hypertrophy/hyperplasia, and who would most likely respond to BT. It would also be valuable to verify that the treatment has produced the desired effect, i.e. the elimination of ASM. To this extent, OCT can image the ASM before and after treatment to verify treatment effectiveness. This is not possible with histology, endobronchial biopsies, or any other currently available technology. With the ability to better localize and verify treatment response, BT may show better effectiveness(12).

One of the major causes of Chronic Obstructive Pulmonary Disease (COPD) is inflammation of the airways(7). However, there is currently no way to assess airway inflammation in COPD. While not directly explored in the current study and not possible across all areas of the lung, inflammation of the airway wall caused by cellular infiltration and cytokine release can lead to thickening of structural components such as the epithelium, the basement membrane, and adventitial layer which could potentially be assessed by our OCT system. OCT imaging could quantify progression of disease and response to therapy with longitudinal measurements of these structural components.

There are some limitations to this study. Each catheter in our 800-nm system is tuned to optimize the imaging of a specific size airway. For example, for this study we optimized the catheters to image the airway wall microstructures of approximately 2 mm airways. In a future study, we optimized the catheter to image the airway wall microstructures of 6 mm in

diameter airways. Thus, each catheter has a limited optimal airway size range for imaging. Second, at the lower extreme, we are currently limited in that the smallest airways we can image are approximately 1.8 mm in diameter; thus, it is difficult to assess airways across all the various diameters found in the lung and disease process that occur beyond our imaging depth in the lung parenchyma. We have begun to test a new micro-OCT catheter that is only 1 mm in diameter(23), which would allow in vivo measurements in the smallest airways where most chronic lung diseases begin(10, 17). Third, OCT imaging of the airways requires bronchoscopy. Bronchoscopy, while commonly performed with few risks and side effects is not completely benign.

In conclusion, we have demonstrated the validity of our 800-nm diffractive high-resolution OCT system to resolve and measure airway wall microstructural components *in vivo*. The ability to acquire microscopic level information of the airways *in vivo* will enhance the ability to diagnose and study lung disease. This technology has the potential to improve prognosis of lung diseases through longitudinal quantification of pathophysiological changes in the airway walls. In addition, it will help guide therapeutic interventions by directly showing the changes in the airways following treatment.

Acknowledgments:

We acknowledge support from Mr. Roberto Zambito for labeling histology.

Funding:

This research was supported in part by the National Institutes of Health (grants R01CA153023 (X.D.L.), R01HL121788 (R.H.B. and X.D.L.), T32HL007534 and F32HL144121 (J.T.), The Wallace H. Coulter Foundation (X.D.L.),

References and Notes:

1. Adams DC, Hariri LP, Miller AJ, Wang Y, Cho JL, Villiger M, Holz JA, Szabari MV, Hamilos DL, Scott Harris R, Griffith JW, Bouma BE, Luster AD, Medoff BD, and Suter MJ. Birefringence microscopy platform for assessing airway smooth muscle structure and function in vivo. Science translational medicine 8: 359ra131, 2016.
2. Adams DC, Miller AJ, Applegate MB, Cho JL, Hamilos DL, Chee A, Holz JA, Szabari MV, Hariri LP, Harris RS, Griffith JW, Luster AD, Medoff BD, and Suter MJ. Quantitative assessment of airway remodelling and response to allergen in asthma. Respirology 24: 1073–1080, 2019. [PubMed: 30845351]
3. Chen Y, Ding M, Guan W, Wang W, Luo W, Zhong C, Jiang M, Jiang J, Gu Y, Li S, and Zhong N. Validation of human small airway measurements using endobronchial optical coherence tomography. Respir Med 109: 1446–1453, 2015. [PubMed: 26427628]
4. Coxson HO, Quiney B, Sin DD, Xing L, McWilliams AM, Mayo JR, and Lam S. Airway wall thickness assessed using computed tomography and optical coherence tomography. Am J Respir Crit Care Med 177: 1201–1206, 2008. [PubMed: 18310475]
5. Fujimoto JG, Brezinski ME, Tearney GJ, Boppart SA, Bouma B, Hee MR, Southern JF, and Swanson EA. Optical biopsy and imaging using optical coherence tomography. Nat Med 1: 970–972, 1995. [PubMed: 7585229]
6. Girodet PO, Allard B, Thumerel M, Begueret H, Dupin I, Ousova O, Lassalle R, Maurat E, Ozier A, Trian T, Marthan R, and Berger P. Bronchial Smooth Muscle Remodeling in Nonsevere Asthma. Am J Respir Crit Care Med 193: 627–633, 2016. [PubMed: 26540234]
7. Global Strategy for the Diagnosis MaPoC, Global Initiative for Chronic Obstructive Lung Disease (GOLD) 2017. Available from: http://goldcopd.org. (Accessed July 19, 2017).

8. Gora MJ, Suter MJ, Tearney GJ, and Li XD. Endoscopic optical coherence tomography: technologies and clinical applications. Biomed Opt Express 8: 2405–2444, 2017. [PubMed: 28663882]
9. Hariri LP, Applegate MB, Mino-Kenudson M, Mark EJ, Bouma BE, Tearney GJ, and Suter MJ. Optical frequency domain imaging of ex vivo pulmonary resection specimens: obtaining one to one image to histopathology correlation. Journal of visualized experiments : JoVE 2013.
10. Hogg JC, Pare PD, and Hackett TL. The Contribution of Small Airway Obstruction to the Pathogenesis of Chronic Obstructive Pulmonary Disease. Physiological reviews 97: 529–552, 2017. [PubMed: 28151425]
11. James AL, Elliot JG, Jones RL, Carroll ML, Mauad T, Bai TR, Abramson MJ, McKay KO, and Green FH. Airway smooth muscle hypertrophy and hyperplasia in asthma. Am J Respir Crit Care Med 185: 1058–1064, 2012. [PubMed: 22403800]
12. Langton D, Wang W, Sha J, Ing A, Fielding D, Hersch N, Plummer V, and Thien F. Predicting the Response to Bronchial Thermoplasty. The journal of allergy and clinical immunology In practice 8: 1253–1260.e1252, 2020. [PubMed: 31712191]
13. Lee AM, Kirby M, Ohtani K, Candido T, Shalansky R, MacAulay C, English J, Finley R, Lam S, Coxson HO, and Lane P. Validation of airway wall measurements by optical coherence tomography in porcine airways. PloS one 9: e100145, 2014. [PubMed: 24949633]
14. Li J, Thiele S, Quirk BC, Kirk RW, Verjans JW, Akers E, Bursill CA, Nicholls SJ, Herkommer AM, and Giessen H. Ultrathin monolithic 3D printed optical coherence tomography endoscopy for preclinical and clinical use. Light Sci Appl 9: 1–10, 2020. [PubMed: 31934333]
15. Li K, Liang W, Mavadia-Shukla J, Park H, Li D, Yuan W, Wan S, and Li X. Super-achromatic optical coherence tomography capsule for ultrahigh-resolution imaging of esophagus. J Biophotonics 12: e201800205, 2019. [PubMed: 30302923]
16. Mavadia-Shukla J, Fathi P, Liang W, Wu S, Sears C, and Li X. High-speed, ultrahigh-resolution distal scanning OCT endoscopy at 800 nm for in vivo imaging of colon tumorigenesis on murine models. Biomedical optics express 9: 3731–3739, 2018. [PubMed: 30338151]
17. Mead J The lung's "quiet zone". The New England journal of medicine 282: 1318–1319, 1970. [PubMed: 5442364]
18. Pahlevaninezhad H, Khorasaninejad M, Huang Y-W, Shi Z, Hariri LP, Adams DC, Ding V, Zhu A, Qiu C-W, and Capasso F. Nano-optic endoscope for high-resolution optical coherence tomography in vivo. Nat Photonics 12: 540–547, 2018. [PubMed: 30713581]
19. Park H, Mavadia-Shukla J, Yuan W, Alemohammad M, and Li XD. Broadband rotary joint for high-speed ultrahigh-resolution endoscopic OCT imaging at 800 nm. Opt Lett 42: 4978–4981, 2017. [PubMed: 29216160]
20. Tearney GJ, Brezinski ME, Bouma BE, Boppart SA, Pitris C, Southern JF, and Fujimoto JG. In vivo endoscopic optical biopsy with optical coherence tomography. Science 276: 2037–2039, 1997. [PubMed: 9197265]
21. Tumlinson AR, Považay B, Hariri LP, McNally JB, Unterhuber A, Hermann BM, Sattmann H, Drexler W, and Barton JK. In vivo ultrahigh-resolution optical coherence tomography of mouse colon with an achromatized endoscope. J Biomed Opt 11: 064003, 2006. [PubMed: 17212526]
22. Xi J, Zhang A, Liu Z, Liang W, Lin LY, Yu S, and Li XD. Diffractive catheter for ultrahigh-resolution spectral-domain volumetric OCT imaging. Opt Lett 39: 2016–2019, 2014. [PubMed: 24686663]
23. Yuan W, Brown R, Mitzner W, Yarmus L, and Li XD. Super-achromatic monolithic microprobe for ultrahigh-resolution endoscopic optical coherence tomography at 800 nm. Nat Commun 8: 1531, 2017. [PubMed: 29142274]
24. Yuan W, Chen D, Sarabia-Estrada R, Guerrero-Cázares H, Li D, Quiñones-Hinojosa A, and Li XD. Theranostic OCT microneedle for fast ultrahigh-resolution deep-brain imaging and efficient laser ablation in vivo. Sci Adv 6: eaaz9664, 2020. [PubMed: 32300661]
25. Yuan W, Mavadia-Shukla J, Xi J, Liang W, Yu X, Yu S, and Li XD. Optimal operational conditions for supercontinuum-based ultrahigh-resolution endoscopic OCT imaging. Opt Lett 41: 250–253, 2016. [PubMed: 26766686]

26. Yun SH, Tearney GJ, Vakoc BJ, Shishkov M, Oh WY, Desjardins AE, Suter MJ, Chan RC, Evans JA, and Jang IK. Comprehensive volumetric optical microscopy in vivo. Nat Med 12: 1429, 2006. [PubMed: 17115049]

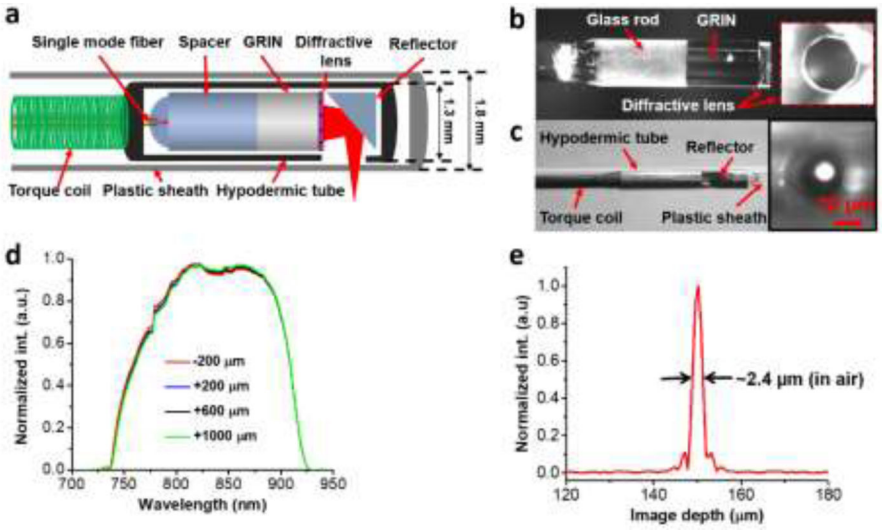

Figure 1:

(a) Schematic of the diffractive OCT catheter. (b) Photo of the assembled distal optics of diffractive OCT catheter, inset shows photo of the diffractive lens. (c) Photo of the assembled diffractive catheter, inset shows image of the focused spot captured by a charge-coupled device (CCD) camera when the catheter was encased with a plastic sheath of a 1.8 mm outer diameter (OD). (d) The back-reflected spectra measured by placing a mirror at different locations relative to the focal plane of the catheter along the imaging depth. The spectra were captured by an optical spectrum analyzer (OSA). (e) The measured point spread function (PSF) with an full-width at half-maximum (FWHM, i.e. axial resolution) of 2.4 μm in air (1.7 μm in tissue) when using a home-made Ti:sapphire laser as the light source.

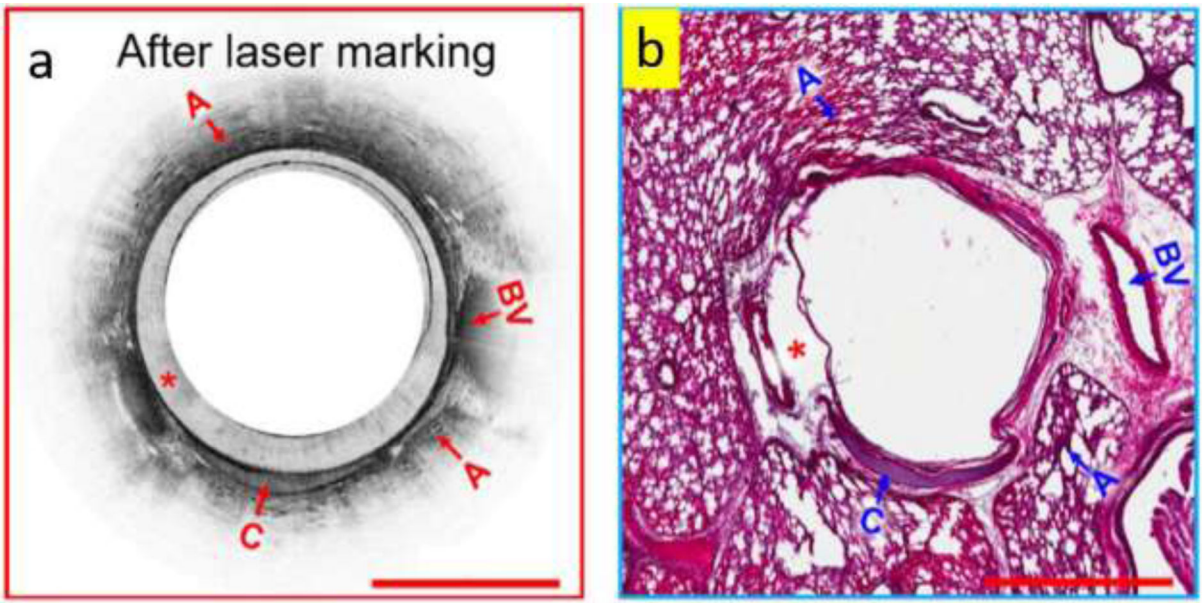

Figure 2:
Example of laser marking (*) of airway on OCT (a) and matched histology (b). A= alveoli, BV = blood vessel, C = cartilage. Scale bars: 1 mm

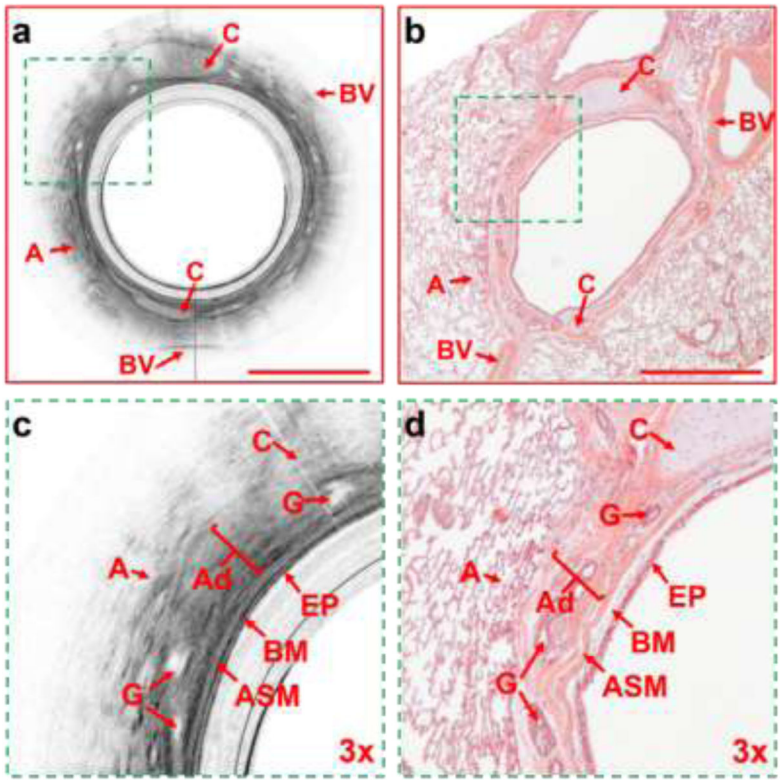

Figure 3:

Representative cross-sectional OCT and histological images. (a) The OCT airway image of the entire matched airway. (b) H & E histological image of the entire matched airway. (c) the 3X enlarged matched area from Figure 3a showing the structural components of the airway wall. (d) the 3X enlarged matched area from Figure 3b showing the matched structural components of the airway wall. A= alveoli, C= cartilage, BV=blood vessel, EP = epithelium, BM = basement membrane, ASM= airway smooth muscle, G = glands, Ad = adventitia. Scale bars: 1 mm.

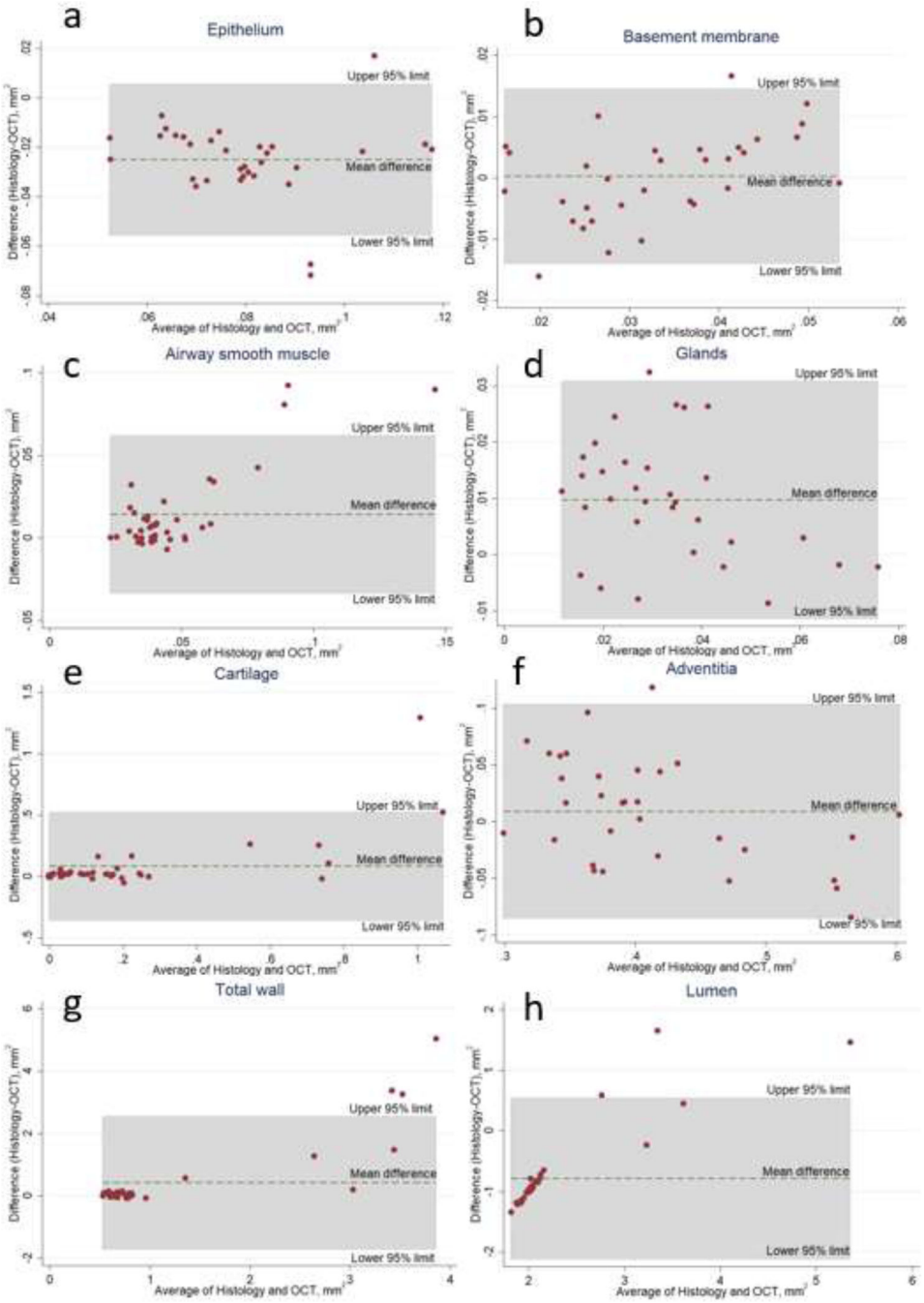

Figure 4:

Bland-Altman plots comparing bias between OCT imaging and histology across the various microstructures of the airway wall. (a) epithelium, (b) basement membrane, (c) airway smooth muscle, (d) glands, (e) cartilage, (f) adventitia, (g) total airway wall, (h) lumen. We observed no system bias among the microstructures measured.

Table 1:

Mean sizes of airway and components measured by OCT and Histology

Structure	OCT	Histology	*p-value
Epithelium (mm^2)	0.092±0.018	0.067±0.017	<0.001
Basement membrane (mm^2)	0.033±0.0093	0.033±0.012	0.57
Airway smooth muscle (mm^2)	0.040±0.014	0.054±0.033	<0.001
Glands (mm^2)	0.028±0.018	0.038±0.015	<0.001
Cartilage (mm^2)	0.20±0.23	0.26±0.37	0.03
Adventitia (mm^2)	0.41±0.094	0.42±0.072	0.17
Total wall (mm^2)	0.91±0.57	1.3±1.5	0.02
Lumen (mm^2)	2.6±0.39	1.8±0.97	<0.001

*paired t-test

Table 2.

Correlation between the OCT and histology measurements

Structure	R	β_0	β_1	*p-value
Epithelium	0.61	0.047	0.67	<0.001
Basement membrane	0.82	0.013	0.60	<0.001
Airway Smooth Muscle	0.76	0.022	0.32	<0.001
Glands	0.80	−0.0092	0.99	<0.001
Cartilage	0.81	0.063	0.47	<0.001
Adventitia	0.86	−0.067	1.1	<0.001
Airway wall	0.76	0.51	0.30	<0.001
Lumen	0.84	2.0	0.34	<0.001

* Linear regression